Tensile properties of melt intercalated polyamide 6 - montmorillonite nano-composites

A.N. Wilkinson, Z. Man, J.L. Stanford, P. Matikainen, M.L. Clemens, G.C. Lees, C.M. Liauw

PII: S0266-3538(07)00137-6
DOI: 10.1016/j.compscitech.2007.03.024
Reference: CSTE 3648

To appear in: *Composites Science and Technology*

Received Date: 16 August 2006
Revised Date: 21 February 2007
Accepted Date: 20 March 2007

Please cite this article as: Wilkinson, A.N., Man, Z., Stanford, J.L., Matikainen, P., Clemens, M.L., Lees, G.C., Liauw, C.M., Tensile properties of melt intercalated polyamide 6 - montmorillonite nanocomposites, *Composites Science and Technology* (2007), doi: 10.1016/j.compscitech.2007.03.024

Tensile properties of melt intercalated polyamide 6 - montmorillonite nanocomposites

A.N. Wilkinson[a]*, Z. Man[a†], J.L. Stanford[a], P. Matikainen[b‡], M.L. Clemens[b], G.C. Lees[b], C.M. Liauw[b]

[a]University of Manchester School of Materials, Materials Science Centre, Grosvenor Street, Manchester, M1 7HS, UK. [b]Dalton Research Institute, Manchester Metropolitan University, Manchester, M1 5GD, UK.

Abstract

The effects of montmorillonite (MMT) addition level on the tensile properties of PA6-MMT polymer-layered silicate nanocomposites (PLSN) were quantified using factorial experimental design (FED) to fit experimental data to a series of polynomial response equations. Tensile behaviour, determined via FED, was related to the morphologies of the PLSN and compared to additional experimental data, determined for both a PLSN produced as a confirmation experiment and a PA6-MMT microcomposite of equivalent MMT content. In general, the PLSN displayed mechanical behaviour in keeping with their mixed exfoliated lamellae/intercalated lamellae-stack composite morphology and with the formation of a continuous phase of constrained polymer at a MMT loading of approximately 4 wt.-%. The data generated by the FED response equation for tensile modulus were compared to the predictions of the Halpin-Tsai composite theory model. A modification to the Halpin-Tsai model was made in order to take account of changes in the distribution of the number (n) of lamellae in the stack particles. Using experimental data for n, the composite moduli of the PLSN were successfully modelled as summations of the contributions of each particle fraction of varying n.

Keywords: A: polymer-matrix composites, nanocomposites. B: mechanical properties.

* Corresponding author. Tel.: +44 161 306 569; fax: +44 161 306 3586;
E-mail address: Arthur.wilkinson@manchester.ac.uk.

† Current address: Universiti Teknologi Petronas, Perak, Malaysia.

‡ Current address: Perlos (Beijing), Beijing, P.R. China.

Introduction

Polymer-layered silicate nanocomposites (PLSN) are formed by the incorporation of only a few weight percent (wt %) of a nanoscale lamellar-silicate filler into a polymer. PLSN offer a number of advantages over traditional polymer composites [1-6], in that significant enhancements in mechanical properties are combined with low density, reduced permeability and increased flammability resistance. These improvements result from the incorporation of thin (≈ 1 nm) silicate lamellae that exhibit both high surface area (up to 10^3 m^2 g^{-1}) and large aspect ratios (often ≥ 100) which, when combined with their high tensile modulus (> 100 GPa), produce efficient reinforcement of a polymer matrix [7-9]. Layered-silicates initially consist of stacks of lamellae (tactoids) which must be exfoliated (delaminated) to release individual lamellae and form a PLSN [10]. However, it is extremely difficult to achieve complete exfoliation and most PLSN contain regions of both exfoliated silicate lamellae and "intercalated" lamellae stacks. These stacks contain intermediate layers comprising mixtures of organic surface treatments for the filler (intercalants) and polymer chains that have diffused into the interlayer spacings between the lamellae [10]. Thus, the degree of exfoliation achieved has significant effects on the surface area, aspect ratio and mechanical properties [8, 9] of the filler particles and therefore tends to dominate the mechanical properties of a PLSN.

An earlier paper from this study [11], described the production of PA6-montmorillonite (MMT) PLSN by melt compounding in a co-rotating twin-screw extruder, and their morphologies were characterised using a range of techniques. This, complementary, paper reports on the tensile properties of those PLSN. Mechanical behaviour is related to the structure of the PLSN described in the preceding paper [11] and compared to the predictions of both standard composite-theory models, and versions modified in order to take account of changes in the distribution of the number of lamellae in intercalated stack particles

Experimental

The particulate composites used were produced from a PA6 melt-compounded with either an unmodified montmorillonite (MMT) or an organo-modified montmorillonite (OMMT) [11].

The PA6 (Akulon F136), supplied by DSM, was a high-viscosity extrusion grade designed for film applications. The unmodified MMT (PGW), supplied by Nanocor, was a high-purity grade. The OMMT (Nanomer 1.30TC), supplied by Nanocor, was an octadecylammonium salt ($C_{18}H_{37}NH^{3+}$) - modified grade developed for extrusion compounding with PA6.

Factorial experimental design (FED) was used to quantify the effects of OMMT addition on the tensile properties of the PA6, using Maximise™ software (BTR Technology). The design chosen was a 3 level full-factorial, with OMMT weight-percentage (wt%) addition as the sole variable at nominal levels of 0, 5 and 10 wt%. FED is usually used to study complex systems in which interactions occur between multiple input variables [12] and, in fact, the results presented in this paper form were extracted from a larger, multivariate study. In this case, FED was used specifically to provide an experimentally efficient method of determining experimental error and of fitting the experimental data, thus allowing the prediction of mechanical properties at intermediate levels of OMMT addition. For comparison, a PGW-based MMT microcomposite was produced at the mid-level of the design (nominally 5 wt% addition – experimentally 4.7 wt% [11]). The composites were identified using a simple coding system consisting of the nominal clay wt.-% followed by T or P, denoting 1.30TC or PGW respectively, as shown in Table 1. In a subsequent compounding experiment, a further PLSN composite - designated 7T - was produced as a confirmation experiment. The reasoning behind this was two-fold: firstly, to assess the accuracy of the FED predictions of mechanical properties at intermediate addition levels of OMMT; and secondly to provide a direct comparison (in terms of wt.-% MMT) to the 5P microcomposite containing unmodified MMT.

Melt compounding was performed using a vented Betol BTS30 co-rotating twin-screw extruder (diameter of screws = 30 mm, length: diameter ratio = 21:1). Dried components (16 hr, 80 ºC) were mechanically premixed then compounded using a screw speed of 40 rpm, a temperature profile of 200 ºC (feed throat) to 220 ºC (die) and a throughput of 8 kg hr^{-1}. The compounds were extruded as twin laces of ≈ 4 mm diameter, which were hauled into a quenching water trough prior to being pelletized. Dried blends (16 hr, 80 ºC) were moulded to

form tensile dumbbells and bar specimens (110 x 10 x 4 mm) using a Boy 15S injection-moulding machine. The barrel temperature profile was 230 ºC (feed throat) to 250 ºC (nozzle) and the mould temperature was maintained at 80 ºC. To minimise moisture uptake moulded specimens were immediately wrapped in aluminium foil and sealed in polyethylene bags. Prior to mechanical testing, all specimens were dried for 6 hours at 80 ºC and then conditioned in a dessicator for a minimum of 3 days. Tensile tests were conducted on moulded dumbbell specimens using a Hounsfield M-series tensometer fitted with an extensometer. Modulus values were determined at a crosshead speed of 1 mm min^{-1}, whilst for the remainder of the test (i.e. beyond 0.5% elongation) a crosshead speed of 50 mm min^{-1} was used.

Results and Discussion

Mechanical Testing

Data derived from mechanical testing of the PA6 matrix and PA6-clay composites are shown in Table 2. To provide a better comparison, the PA6 specimens used for testing were injection moulded from material that had undergone the same twin-screw extrusion procedure as the PA6-clay composites. Using FED software the experimental data were fitted to a set of polynomial response equations of the form

$$f(x) = A_0 + A_1 x + A_2 x^2 \qquad (1)$$

where f(x) is the mechanical property response considered, and A_0, A_1 and A_2 are the respective coefficients for the response mean and the linear and non-linear effects of changing the clay level (x). Using a statistical t-test, the coefficients for all responses were found to be of ≥ 95% significance level and therefore were deemed to be statistically significant. The outputs from the response equations determined for tensile properties are shown in Figures 1-2, in comparison to both the experimental data used to generate the curves, the 5P microcomposite and the 7T PLSN produced as a confirmation experiment. In the figures actual MMT content, as measured by ashing [11], is used rather than OMMT addition level.

Figure 1 shows the development in tensile modulus for addition levels of MMT between 0 and 7.5 wt%. As expected, the fit of the FED response equation to the experimental data is good, in that the greatest deviation of the experimental data from the FED response curve (≈ 400 MPa at 3.3 wt% MMT) was estimated as being not statically significant; i.e. having < 95 % significance in a t-test using a value of percentage standard deviation for the predicted value (calculated from the response equation) identical to that determined experimentally for the 5T compound. Similarly, the confirmation experiment showed that the difference between the predicted value from the response equation and the experimental modulus value of the 7T PLSN (8542 MPa) was not statistically significant. In general, the response curve is observed to rise sharply at low levels of clay addition, with a modulus ratio of 1.7 (i.e. a 70% increase relative to the PA6 matrix) being achieved after the addition of only 3.75 wt% MMT (≈ 5.4 wt% of 1.30TC OMMT). The rise in modulus upon further clay addition is less significant, with modulus ratio increasing from 1.7 to ≈ 1.9 as MMT content increases from 3.75 to 7.50 wt%. Reductions in modulus enhancement at higher levels of OMMT addition have been reported in other studies [9, 13 - 15] and have been ascribed to reduced levels of exfoliation [15]. These reductions result from lamella-orientation effects, as the rising number of particles increasingly interact with each other generating packing constraints [10]. Thus, above a critical loading of MMT, proposed to be ≤ 5 wt% for MMT lamellae with aspect ratios of ≥ 100 [7], these constraints are predicted to result in the formation of an ordered nematic phase [16]. The XRD data for these PLSN reported previously [11] did indicate that a more ordered, intercalated structure had developed in the PLSN as the MMT content was raised from 3.3 to 7.2 wt%. In addition, measurements of particle dimensions from TEM images [11] showed that the 5T PLSN exhibited a mean value of 1.8 silicate lamellae per particle, resulting from a particle distribution comprising a predominance of exfoliated lamellae together with a minority of intercalated lamella stacks containing between 2 and 6 lamellae. In contrast, the 10T PLSN exhibited a mean value of 3.8 silicate lamellae per particle [11], resulting from a particle distribution comprising a

predominance of intercalated lamella stacks containing between 2 and 10 lamellae. These intercalated silicate-lamellae stacks will have significantly lower moduli than the ≥ 178 GPa reported for exfoliated, individual silicate lamellae [7-9] as a result of the low-modulus gallery layers, comprising mixtures of octadecylammonium-salt intercalant and intercalated PA6 chains.

Overall, Figure 1 shows the incorporation of OMMT to have resulted in significant enhancement of the modulus of the PA6 matrix. In comparison, modulus-ratio values of ≈1.9 have been reported for PA6-glass fibre composites [17] but only at addition levels of ≥ 18 wt%. In the same study [17], 10 wt% of glass fibres gave values of modulus ratio ≈1.3. Thus, the modulus ratio of 1.34 exhibited by the 5P microcomposite containing 4.7 wt % MMT appears excellent in comparison to the value for a glass-fibre composite, but is still significantly lower than the value of 1.78 predicted for a PLSN at 4.7 wt % MMT by the FED response equation and well below the experimental value of 1.85 measured for the 7T PLSN (4.8 wt % MMT).

During tensile testing several deformation behaviours were observed. The PA6 matrix exhibited an extrinsic yield-point at approximately 4% strain followed by a significant degree of post-yield drawing before fracture occurred at approximately 47% strain. However, the addition of 1.30TC OMMT inhibited yielding to such an extent that the 5T PLSN failed immediately after yielding, at a reduced strain level of approximately 3%, and the 7T and 10T PLSN exhibited brittle fracture at low strains (< 2%) without exhibiting any distinct yielding. The addition of PGW unmodified-MMT inhibited yielding to a much lesser extent and some post-yield drawing was observed for the 5P microcomposite, although elongation at break (11.6%) was much lower than the PA6 matrix. Due to these differences in deformation behaviour, maximum tensile stress was chosen as the FED response, which relates to values of yield-stress for the PA6 matrix and 5T PLSN, and to values of stress-at-break for the 10T and 7T PLSN. Figure 2 shows the development in maximum tensile stress for addition levels of MMT between 0 and 7.5 wt%. The fit of the FED response equation to the experimental data is excellent, and there is good agreement between the predicted value from the response equation and the experimental stress

value of the 7T PLSN (92.7 MPa) produced as a confirmation experiment. Maximum tensile stress is observed to increase by ≈30% upon the addition of 4 wt% MMT (i.e. stress ratio rises to ≈ 1.3), then to drop at an equivalent rate upon further addition of MMT before returning to approximately the same value as the PA6 matrix at 7.5 wt% MMT. The increase in yield stress up to ≈ 5 wt% MMT may be ascribed to an increase in the constrained volume of polymer [15, 18]. This volume is dependent on the polymer-filler interfacial area, which rises rapidly with OMMT addition up to a critical loading of MMT, where packing constraints result in the formation of an ordered nematic phase [10, 16]. It has been proposed [18-20] that at this critical MMT loading a continuous phase of constrained polymer forms, via coalescence of the interfacial regions of the closely packed lamellae. Dynamic mechanical studies of the 5T and 10T PLSN, reported previously [11], showed strong indications of the formation a continuous phase of constrained polymer. This morphological change will significantly affect the deformation behaviour of the PA6 matrix, as this continuous phase will presumably consist of a mixture of constrained amorphous chain-segments [21-23] and γ-phase crystallites [24, 25] – both of which will exhibit much lower ductility than the unconstrained amorphous chain-segments in PA6. Thus, the distinct change in deformation behaviour at intermediate levels of MMT may result from the formation of this continuous phase of constrained polymer and the consequent inhibition of bulk plastic-yielding of the PA6 matrix. At levels of >5 wt% MMT the, now, non-yielding PLSN exhibit a reduction in stress-at-break with increasing levels of filler addition - behaviour that is typical of particulate-filled polymer microcomposites [26].

Studies of the tensile behaviour of PA6 PLSN typically report that bulk yielding is not inhibited [13, 27 - 29]. However, the reported increases in yield stress usually tend to asymptote at addition levels of OMMT that vary between 2 and 10 wt% [13, 27, 28] or, less commonly, yield stress decreases at high levels of OMMT addition [29]. In comparison to the stress ratio levels achieved by PA6-glass fibre (PA6-GF) composites, PLSN tend to perform very well at low levels of OMMT addition. For example: a stress ratio of 1.42 was reported [30] for a PA6 PLSN containing 3.0 wt% MMT, compared to ratios of 1.17, 1.52 and 1.86 for PA6-GF

composites containing 10, 20 and 30 wt% glass fibres, respectively. Similarly, Cho and Paul [27] report a stress ratio of 1.30 for a PA6 PLSN containing 3.16 wt% MMT (≈ 5 wt% OMMT), compared to ratios of 1.18 and 1.13 for a PA6 microcomposite containing 5 wt% MMT and a PA6-GF composite containing 5 wt% glass fibres, respectively. Figure 2 shows the 5P microcomposite containing 4.7 wt% MMT to exhibit a stress ratio of ≈ 1.1. Thus, addition of low levels of unmodified MMT appear to result in similar stress enhancement to equivalent levels of glass fibres, as was shown earlier for tensile modulus.

Composite Models

In order to better understand the reinforcing effects of MMT on the PA6 matrix, the predictions of several composite theory models were compared to the results of the FED response equation for the tensile modulus of the PLSN. Halpin-Tsai theory [31] is the most widely applied composite model for the prediction of the moduli of PLSN as a function of aspect ratio [7-9], and is given as

$$\frac{E_c}{E_m} = \frac{1 + \zeta\eta\phi_f}{1 - \eta\phi_f} \qquad (2)$$

where E_c and E_m represent the composite and matrix moduli, respectively, ζ is a shape factor dependent upon filler geometry and loading direction, ϕ_f is the volume fraction of the filler and η is given by

$$\eta = \frac{E_f / E_m - 1}{E_f / E_m + \zeta} \qquad (3)$$

where E_f represents the modulus of the filler.

In this study, the value of ζ was taken as twice the aspect ratio of the reinforcing particles, i.e. $\zeta = 2(l/t)$ where l and t are the length and thickness of the silicate lamellae or the lamellae-stacks. There are a number of assumptions inherent in the use of Equation 2: (i) the properties of both the matrix PA6 and the MMT within the PLSN are identical to those of the pure materials; (ii) the PA6 and MMT lamellae are linear elastic, isotropic and perfectly bonded; (iii) the MMT

lamellae are perfectly aligned, asymmetric and uniform in shape and size. Obviously, these simplifying assumptions will result in disparities between the predictions of the Halpin-Tsai theory and the behaviour of real, more complex, systems such as PLSN [7-9]. These disparities will be discussed in the sections that follow.

As $\zeta \rightarrow \infty$, Equation 2 reduces to the parallel (isostrain) model of the rule-of-mixtures (given in Equation 4) and, conversely, as $\zeta \rightarrow 0$ Equation 2 reduces to the series (isostress) model of the rule-of-mixtures (Equation 5). Thus, Equations 4 and 5 provide the upper and lower bounds of modulus prediction, respectively.

$$E_c = \phi_f E_f + (1 - \phi_f) E_m \qquad (4)$$

$$\frac{1}{E_c} = \frac{\phi_f}{E_f} + \frac{(1 - \phi_f)}{E_m} \qquad (5)$$

Figure 3 shows the effects of filler volume fraction (ϕ) and aspect (l/t) ratio on the modulus of a PLSN. The values of E_m and E_f used in the calculations were 4.62 GPa for the PA6 matrix (Table 1) and 178 GPa, the most widely reported value for a silicate lamella [32]. The solid lines marked P and S indicate upper and lower bounds calculated using the parallel and series models (Equations 4 and 5) respectively. The dashed lines are Halpin-Tsai calculations (Equation 2) using values of aspect ratio between 20 and 200. In this case the PLSN are considered to be completely exfoliated, the reduction in modulus due to the presence of intercalated silicate-lamellae stacks is considered later. Figure 3 shows the Halpin-Tsai calculation at an aspect ratio of 200 to be close to the upper bound calculated using the parallel model (Equation 4). The slopes of the calculated lines then decrease significantly as the aspect ratio is reduced to 20. The open symbols in Figure 3 indicate the FED tensile-modulus response equation (from Figure 1). Surprisingly, the initial response-equation points rise above the P-curve until approximately ϕ = 0.014. This indicates that the real values of either E_f or E_m, or both, may be higher than the values used in generating Figure 3. From $\phi \approx 0.008$ the slope of the response-equation curve decreases rapidly; at values of $\phi > 0.014$ the points lie below the P-curve and the curve

essentially asymptotes by $\phi \approx 0.025$. Using Equation 4, the initial response-equation data between $0 \leq \phi \leq 0.005$ were fitted to the parallel model, giving a value of E_f of ≈ 250 GPa (for $E_m = 4.62$ GPa). A similar fit was performed over the same range of volume fraction (0.005) between $0.025 \leq \phi \leq 0.030$. Extrapolation to $\phi = 0$ gave a value of $E_m \approx 7.9$ GPa and, using this value of E_m, the rule of mixtures fit gave a value of $E_f \approx 35$ GPa. These fits to the curve raise a number of points: (i) the modulus value of 178 GPa for an exfoliated silicate lamella may be too low; (ii); the modulus of the silicate reinforcement appears to drop significantly at values of $\phi >$ 0.014; (iii) composite theory assumes the modulus of the matrix to be the same as the unfilled polymer. However, the introduction of a huge surface area of high surface-energy silicate into the PA6 will result in a considerable increase in the volume of constrained polymer chain segments, both in the amorphous phase and in the volume of γ-phase crystallites, which will tend to increase the value of E_m.

Based on molecular dynamics simulations [33], Manevitch and Rutledge reported a value of ≈ 250 Nm^{-1} for the membrane-modulus of a silicate lamella [9, 33]. Dividing this value by the thickness of a silicate lamella (0.94 nm [8]) gives a value of $E_f = 266$ GPa. This value is very close to the value of $E_f \approx 250$ GPa determined from the fit of the parallel model to the initial response-equation data in Figure 3. However, it should be noted that Manevitch and Rutledge [33] also calculated a smaller value for the thickness of a silicate lamella of 0.615 nm, giving a value of $E_f \approx 400$ GPa. The modulus value of a smectite clay lamella is a subject of debate. Chen and Evans [32] surveyed the published estimates of elastic moduli, reporting both a convergence of opinion in the range 178-265 GPa and that a value of 400 GPa appeared rather high when compared to the density dependence of modulus for silica and aluminosilicates.

Figures 4 and 5 both show the effects of filler volume fraction (ϕ) and aspect (l/t) ratio on the calculated modulus of a PLSN. The value of E_m used in the calculations for both Figure 4 and 8 was $E_m = 4.62$ GPa and the values of E_f used were 265 and 400 GPa for Figure 7 and 8, respectively. The use of these higher values for E_f increases the gradients of the calculated E_c/E_m

versus ϕ lines, compared to Figure 6. Thus, in both Figure 4 and 5 the response-equation curve now lies within the upper and lower bounds defined by the parallel and series models, respectively. Measurements from TEM micrographs [11] gave mean values of particle length of 143 and 164 nm for the 5T and 10T PLSN, for which $\phi = 0.0134$ and 0.0301, respectively. Given that TEM also showed the 5T PLSN to contain mainly exfoliated silicate lamellae, it may be expected that PLSN produced within the range $0 < \phi \leq 0.01$ will be highly exfoliated, resulting in high aspect (l/t) ratios, as 143 nm / 0.94 nm ≈ 150. In Figure 4, where $E_f = 265$ GPa, the response-equation curve up to $\phi = 0.01$ essentially lies on, or between, the lines calculated for aspect ratios of 200 and 100 whereas in Figure 5, where $E_f = 400$ GPa, the initial response-equation curve follows the line for an aspect ratio of 50. Thus, at first sight the value of $E_f = 400$ GPa used to generate Figure 5 would appear to be too high. However, it has been assumed in these calculations that all the particles within the PLSN are exfoliated silicate lamellae, whereas TEM has shown both the 5T and 10T PLSN to contain a mixture of exfoliated lamellae and lamellae-stacks [11].

The tensile modulus, E_{stack}, of a lamellae stack parallel to the lamellae may be estimated using a parallel model [7, 8], similar to Equation 4; i.e.

$$E_{Stack} = \phi_{MMT} E_{MMT} + \phi_{Gallery} E_{Gallery} \qquad (6)$$

where ϕ_{MMT} and E_{MMT} are, respectively, the volume fraction of MMT lamellae in the stack and the modulus of a MMT lamella, and $\phi_{Gallery}$ and $E_{Gallery}$ are, respectively, the volume fraction of gallery space in the stack and the modulus of the material in the gallery. The value of $\phi_{Gallery}$ may be expressed, in terms of X-ray d-spacings, as [7, 8]

$$\phi_{Gallery} = \frac{(n-1)(d_{001} - t_{lam})}{d_{001}(n-1) + t_{lam}} \qquad (7)$$

where n is the number of lamellae per stack, d_{001} is the repeat spacing between silicate lamellae and t_{lam} is the thickness of a silicate lamella. Figure 6 shows the effect of increasing the number (n) of silicate lamellae in a stack on the modulus of the stack. Two curves are shown, one for

d_{001} = 3.4 nm and the other for d_{001} = 3.8 nm, as these values approximate to the d-spacings measured [11] for the 5T and 10T PLSN, respectively. The two curves are very similar, in that both exhibit abrupt drops in modulus as *n* increases from 1 to 2 and eventually asymptote at approximately 70-80 GPa. The average values of *n* for the 5T and 10T PLSN are 1.8 and 3.8, calculated from TEM measurements of particle thickness [11], which equate to values of E_{stack} of ≈ 150 and ≈ 80 GPa for 5T and 10T, respectively. Thus, the reduction in modulus of the reinforcing particles in a PLSN due to the formation of intercalated lamellae-stacks makes the adoption of a value of 400 GPa for the modulus of a silicate lamella more feasible. These significant reductions in modulus result from the low-modulus gallery layers, comprising mixtures of octadecylammonium-salt intercalant and intercalated PA6 chains. The curves in Figure 6 were calculated using a value of $E_{gallery}$ = 4 GPa, i.e. equivalent to the modulus of the PA6 matrix. However, it should be noted that the curves show negligible differences upon reducing $E_{gallery}$ by an order of magnitude to 0.4 GPa.

Figure 7 shows the effect on composite modulus of the number (*n*) of lamellae in a stack. The solid lines marked P and S once again indicate upper and lower bounds calculated using Equations 4 and 5, respectively. The dashed lines are Halpin-Tsai calculations (Equation 2) using a median value of particle length of l_p = 153 nm (experimental values of l_p [11] were 143 and 164 nm for 5T and 10T, respectively) and values of E_f which range from completely exfoliated silicate lamellae (i.e. *n* = 1, E_f = 400 GPa) to lamellae-stacks containing increasing numbers of lamellae (i.e. values of E_{Stack} calculated using Equation 6). The data points generated by the FED response equation lie mainly between the lines corresponding to 1 and 2 lamellae per stack, which corresponds well with the experimentally-determined average of $n_{average}$ = 1.8 for the 5T PLSN at ϕ = 0.0134. For values of $\phi \geq 0.03$, the response-equation data lie on or between the lines corresponding to 2 and 3 lamellae per stack, which corresponds better with the value of $n_{average}$ = 3.8 for the 10T PLSN at ϕ = 0.0301.

It is clear that the calculated lines in Figure 7 correlate much better with the FED response data at low values of ϕ, where a higher level of exfoliation occurs. However, the simple composite models used to generate Figure 7 fail to fit the asymptotic curve of the FED response equation for tensile modulus. The significant reduction in modulus enhancement at particle levels of $\phi \geq 0.015$ may result from a number of factors. Firstly, simple composite models assume the reinforcing particles to be uniform in shape and size, whereas in PLSN as ϕ is increased packing restraints will restrict the degree of exfoliation and consequently increase both the number of silicate-lamellae stacks and the number (n) of lamellae in the stacks. These stacks will significantly reduce reinforcement efficiency due not only to their low modulus, as shown in Figure 6, but also to their lower aspect ratio and reduced efficiency of load transfer from the matrix [8]. Secondly, at higher ϕ there is an increased tendency for particles to overlap, which has been proposed to significantly reduce the efficiency of load transfer between the matrix and the reinforcing particles [9]. Thirdly, simple models neglect other factors such as variations in particle orientation, increased particle attrition at higher ϕ, and changes to the properties of the matrix. In reality, PLSN are complex composite materials composed of a matrix, comprising two polymer phases (i.e. the constrained amorphous/crystalline and the unconstrained amorphous), which encapsulates large numbers of reinforcing particles – both exfoliated lamellae and intercalated stacks - possessing distributions of size, shape and structure as well as variations in orientation. Thus, models such as those used to generate Figure 7, can only give a general, albeit useful, indication of the effects of MMT on the modulus of a PLSN.

One modification to the basic Halpin-Tsai approach that may be useful for PLSN is to take account of the distribution in the number (n) of lamellae in the stack particles. The preceding paper in this study [11] presented histograms, for both the 5T and 10T PLSN, showing the distributions in n calculated using measurements of particle thickness (t_p) from TEM micrographs. These TEM data were used to determine the relative fractions of MMT composed of exfoliated lamellae (i.e. $n = 1$) and of stacks of increasing values of n. Using values of E_{stack}

(calculated using Equation 6) the Halpin-Tsai equation (Equation 2) was used to calculate the contribution of each MMT particle-fraction to E_c, whilst adjusting ϕ_f to account for interlayer thickness and ζ to account for the increase in t_p (as $\zeta = 2\, l_p/t_p$). Thus, E_c is calculated as a summation of the contributions of each particle fraction of varying *n*. Figure 8 shows the effect of the distribution in *n* on the modulus values calculated for the 5T and 10T PLSN, using both the Halpin-Tsai and parallel models (Equations 2 and 4, respectively). The two curves connecting the data points from the models are seen to diverge with increasing MMT content. In particular, at $\phi > 0.0125$ the H-T curve begins to asymptote and the degree of divergence from the P-model curve increases significantly. Consequently, whereas the experimental data for the 5T and 7T PLSN lie approximately midway between the two curves, the experimental value for 10T lies closer to the H-T curve. Thus, the modified HT model gives a good description of the general behaviour of these PLSN.

Conclusions

The response equations for tensile modulus and maximum tensile strength exhibited reduced property enhancement at levels of MMT content ≥ 4 wt%. These property changes may be explained by two effects; firstly, a reduction in the degree of exfoliation due to by lamella packing constraints and, secondly, the formation of a continuous phase of constrained polymer at this MMT loading.

In order to better understand the reinforcing effects of MMT in the PA6 PLSN, the predictions of several composite theory models were compared to the results of the FED response equation for the tensile modulus. Initial plots of the Halpin-Tsai and parallel composite models indicated that the widely-used value of 178 GPa for the modulus of an individual (exfoliated) silicate lamella may be too low, and that the modulus of the reinforcing particles appeared to drop significantly at values of $\phi > 0.014$. Similar plots were produced using a modulus value of 400 GPa calculated by Manevitch and Rutledge [33] which, at first sight, indicated that this value may be too high. Subsequently, useful results were obtained upon

taking account of the mixed exfoliated lamellae/lamellae stack morphology of the PLSN by calculating the tensile moduli of the lamellae stacks using a simple parallel model. However, both the Halpin-Tsai and parallel composite models are linear over the experimental range of $0 \leq \phi \leq 0.04$ and they therefore failed to fit the curve generated by the FED response equation which asymptotes at values of $\phi > 0.014$, indicative of a significant drop in the apparent modulus of the reinforcing particles. Consequently, a modification was made to the basic Halpin-Tsai approach, in order to take account of changes in the distribution in the number (n) of lamellae in the stack particles, in which E_c was calculated as a summation of the contributions of each particle fraction of varying n. This modified model followed the asymptotic behaviour of the FED response equation and provided a good description of the general behaviour of these PLSN.

Acknowledgements

The authors would like to acknowledge Dow Corning for financing this project and DSM and Nanocor for supplying materials.

References

1. Giannelis EP. Polymer layered silicate nanocomposites. Adv. Mater. 1996; 8: 29-35.

2. LeBaron PC, Wang Z, Pinnavaia TJ. Polymer-layered silicate nanocomposites: an overview. Appl. Clay Sci. 1999; 15: 11-29.

3. Alexandre M, Dubois P. Polymer-layered silicate nanocomposites: preparation, properties and uses of a new class of materials. Materials Sci. Eng. 2000; 28: 1-63.

4. Ray SS, Okamoto M. Polymer/layered silicate nanocomposites: a review from preparation to processing. Prog. Polym. Sci. 2003; 28: 1539-1641.

5. Messermith PB, Giannelis EP. Synthesis and barrier properties of poly(ε-caprolactone)-layered silicate nanocomposites. J. Polym. Sci. Part A: Polym. Chem. 1995; 33: 1047-1057.

6. Gilman JW. Flammability and thermal stability studies of polymer layered-silicate (clay) nanocomposites. Appl. Clay Sci. 1999; 15: 31-49.

7. Brune DA, Bicerano J. Micromechanics of nanocomposites: comparison of tensile and compressive elastic moduli and prediction of effects of incomplete exfoliation and imperfect alignment on modulus. Polymer 2002; 43: 369-387.

8. Fornes TD, Paul DR. Modeling properties of nylon 6/clay nanocomposites using composite theories. Polymer 2003; 44: pp 4993-5013.

9. Sheng N, Boyce MC, Parks DM, Rutledge GC, Abes JL, Cohen RE. Multiscale micromechanical modelling of polymer/clay nanocomposites and the effective clay particle. Polymer 2004; 45: 487-506.

10. Vaia RA. Structural characterisation of polymer-layered silicate nanocomposites. In: Pinnavaia TJ, Beall GW, editors. Polymer clay nanocomposites. Chichester: J Wiley & Sons, 2000. pp 229-266.

11. Wilkinson AN, Man Z, Stanford JL, Matikainen P, Clemens ML, Lees GC, Liauw CM. Structure and Dynamic Mechanical Properties of Melt Intercalated PA6-Montmorillonite Nanocomposites. Macromol. Mater. Eng. 2006; 291: 917-928.

12. Montgomery DC. Design and analysis of experiments, 5th ed. New York: J Wiley & Sons, 2001 (chapter 1).

13. Liu L, Qi Z, Zhu X. Studies on Nylon 6/clay nanocomposites by melt-intercalation process. J. Appl. Polym. Sci. 1999; 71:1133-1138.

14. Ma CCM, Kuo CT, Kuan HC, Chiang CL. Effects of swelling agents on the crystallisation behaviour and mechanical properties of polyamide 6/clay nanocomposites. J. Appl. Polym. Sci. 2003; 88:1686-1693.

15. Burnside SD, Giannelis EP. Nanostructure and properties of polysiloxane-layered silicate nanocomposites. J. Polym. Sci. Part B: Polym. Phys. 2000; 38: 1595-1604.

16. Balazs A, Ginzburg VV, Lyztskaya Y, Singh C, Zhulina E. Modeling the phase behaviour of polymer-clay nanocomposites. In: Pinnavaia TJ, Beall GW, editors. Polymer clay nanocomposites. Chichester: J Wiley & Sons, 2000. pp 281-314.

17. Tucker CL III, Liang E. Stiffness predictions for unidirectional short-fiber composites: review and evaluation. Compos. Sci. Technol. 1999; 59: 655-671.

18. Beall GW. New conceptual model for interpreting nanocomposite behaviour. In: Pinnavaia TJ, Beall GW, editors. Polymer clay nanocomposites. Chichester: J Wiley & Sons, 2000. pp 267-280.

19. Maiti P, Okamoto M. Crystallisation controlled by silicate surfaces in Nylon 6-clay nanocomposites. Macromol. Mater. Eng. 2003;288:440-445.

20. Miltner HE, Van Assche G, Pozsgay A, Pukánszky B, Van Mele B. Restricted chain segment mobility in poly(amide) 6/clay nanocomposites evidenced by quasi-isothermal crystallization. Polymer 2006; 47: 826-835.

21. Kojima Y, Usuki A, Kawasumi M, Okada A, Fukushima Y, Kurauchi T, Kamigaito O. Mechanical properties of nylon 6-clay hybrid. J. Mater. Res. 1993; 8: 1185-1189.

22. Kojima Y, Usuki A, Kawasumi M, Okada A, Kurauchi T, Kamigaito O. Sorption of water in Nylon 6-clay hybrid. J. Appl. Polym. Sci. 1993; 49: 1259-1264.

23. Shelley JS, Mather PT, DeVries KL. Reinforcement and environmental degradation of Nylon 6/clay nanocomposites. Polymer 2001; 42: 5849-5858.

24. Lincoln DM, Vaia RA, Wang ZG, Hsiao BS. Secondary structure and elevated temperature crystallite morphology of Nylon 6/layered silicate nanocomposites. Polymer 2001; 42: 1621-1631.

25. VanderHart DL, Asano A, Gilman JW. Solid-state NMR investigation of paramagnetic Nylon-6 clay nanocomposites. 1. crystallinity, morphology and the direct influence of Fe^{3+} on nuclear spins. Chem. Mater. 2001; 13: 3781-3795.

26. Utracki LA, Vu-Khanh T. Filled polymers. In Miles IS, Rostami S, editors. Multicomponent polymer systems. Harlow: Longman, 1992. pp247-257.

27. Cho JW, Paul DR. Nylon 6 nanocomposites by melt compounding. Polymer 2001; 42: 1083-1094.

28. Fornes TD, Yoon PJ, Keskkula H, Paul DR. Nylon 6 nanocomposites: the effect of matrix molecular weight. Polymer 2001; 42: 9929-9940.

29. Wu S., Jiang D, Ouyang X, Wu F, Shen J. The structure and properties of PA6/MMT nanocomposites prepared by melt compounding. Polym. Eng. Sci. 2004; 44: 2070-2074.

30. Wu SH, Wang FY, Ma CCM, Chang WC, Kuo CT, Kuan HC, Chen WJ. Mechanical, thermal and morphological properties of glass fiber and carbon fiber reinforced polyamide-6 and polyamide-6/clay nanocomposites. Mater. Let. 2001; 49: 327-333.

31. Halpin JC, Kardos, JL. The Halpin-Tsai equations: a review. Polym. Eng. Sci. 1976; 16: 344-352.

32. Chen B, Evans JRG. Elastic moduli of clay platelets. Scripta Materialia 2006; 54: 1581-1585.

33. Manevitch OL, Rutledge GC. Elastic properties of a single lamella of montmorillonite by molecular dynamics simulation. J. Phys. Chem. B 2004; 108: 1428-1435.

Figure captions

Figure 1 Tensile modulus versus wt%MMT for the PA6-clay composites. The data points are experimental data for the PA6 matrix (0 wt% MMT), the 5T, 7T and 10T 1.30TC OMMT-based PLSN containing 3.3, 4.8 and 7.2 wt% MMT, respectively, and the 5P microcomposite containing 4.7 wt% of PGW unmodified MMT. The line is generated by the FED response equation. The right-hand axis gives the ratio of modulus values on the left-hand axis to the experimental value determined for the PA6 matrix, and is designed to emphasise the changes resulting from MMT addition. The error bars marked on the points are 95% confidence limits.

Figure 2 Maximum tensile stress versus wt%MMT for PA6-clay composites. The line is generated by the FED response equation and the points are as explained in the caption for Figure 1. The experimental stress ratio is the ratio of stress values on the left-hand axis to the experimental value determined for the PA6 matrix. The error bars marked on the points are 95% confidence limits.

Figure 3 Effects of filler volume fraction (ϕ) and aspect (l/t) ratio on the modulus of a PLSN. Using a value of E_f = 178 GPa, the solid lines P and S were calculated using Equations 4 and 5, respectively. Similarly, the dashed lines are Halpin-Tsai calculations calculated using Equation 2 for values of aspect ratio between 20 and 200. The data shown as open points were generated by the FED response equation. The lines marked Fit (a) and Fit (b) are fits to Equation 4, as explained in the text.

Figure 4 Effects of filler volume fraction (ϕ) and aspect (l/t) ratio on the modulus of a PLSN. Using a value of E_f = 265 GPa, the solid lines P and S were calculated using Equations 4 and 5, respectively. Similarly, the dashed lines are Halpin-Tsai calculations calculated using Equation 2 for values of aspect ratio between 20 and 200. The data shown as open points were generated by the FED response equation.

Figure 5 Effects of filler volume fraction (ϕ) and aspect (l/t) ratio on the modulus of a PLSN. Using a value of E_f = 400 GPa, the solid lines P and S were calculated using Equations 4 and 5, respectively. Similarly, the dashed lines are Halpin-Tsai calculations calculated using Equation 2 for values of aspect ratio between 20 and 200. The data shown as open points were generated by the FED response equation.

Figure 6 Silicate-lamellae stack modulus (E_{Stack}) versus the number of lamellae (n) in a stack. The two curves shown, for d_{001} = 3.4 nm and d_{001} = 3.8 nm, approximate to the d-spacings measured for the 5T and 10T PLSN, respectively.

Figure 7 The effect on composite modulus of the number of lamellae (n) in a stack. The solid lines marked P and S indicate upper and lower bounds calculated using the parallel and series models. The dashed lines are Halpin-Tsai calculations using values of E_f which range from completely exfoliated silicate lamellae (n = 1, E_f = 400 GPa) to lamellae-stacks containing increasing numbers of lamellae (E_{Stack} calculated using Equation 6). The data shown as open points were generated by the FED response equation.

Figure 8 The effect on composite modulus of the distribution of the number of lamellae (*n*) in a stack. The data shown as open squares are experimental values of modulus (Table 2) and the open circle data points are generated by the FED response equation. The two, closed circle, data points for the 5T and 10T PLSN are Halpin-Tsai calculations utilising TEM data of distributions in *n* [11] to give E_c as a summation of the contributions of each particle fraction of varying *n*. Similarly, the closed squares indicate calculations using the parallel model to give E_c as a summation of the contributions of particle fractions of varying *n*. The lines connecting the closed points are purely guides to the eye.

Table 1 Compositional data for the composite samples determined from TGA and ashing [11].

Sample Code[a)]	5T	7T	10T	5P
Nominal wt.-% MMT[b)]	3.5	4.9	7.0	5.0
wt.-% MMT	3.3 (0.2)[c)]	4.8 (0.8)	7.2 (0.9)	4.7 (0.8)
vol.-% MMT[d)]	1.3 (0.1)	1.97 (0.2)	3.0 (0.4)	1.9 (0.3)

[a)] Number is nominal wt.-% clay addition.

[b)] Nominal wt.-% clay addition corrected for 30 wt.-% content of organo-modifier.

[c)] Standard deviation in parentheses.

[d)] Calculated using 2.83 and 1.13 g cm^{-3}, respectively, .for the densities of MMT and PA6.

Table 2 Tensile property data for the PA6 matrix and clay-composites.

Sample	Tensile Modulus /MPa	Yield Stress /MPa	Elongation At Break /%	Stress At Break /MPa
PA6 Matrix	4621 (212)[a)]	76.0 (0.2)	47.2 (7.1)	46.8 (1.5)
5T PLSN	7997 (784)	97.2 (0.7)	3.34 (0.05)	96.9 (0.9)
10T PLSN	8676 (1043)	No Yield	1.50 (0.04)	79.8 (2.3)
5P microcomposite	6168 (896)	82.8 (0.4)	11.6 (1.17)	65.9 (3.3)
7T PLSN	8542 (908)	No Yield	1.92 (0.05)	92.7 (1.1)

[a)] Standard deviations in parentheses.

Fig 1

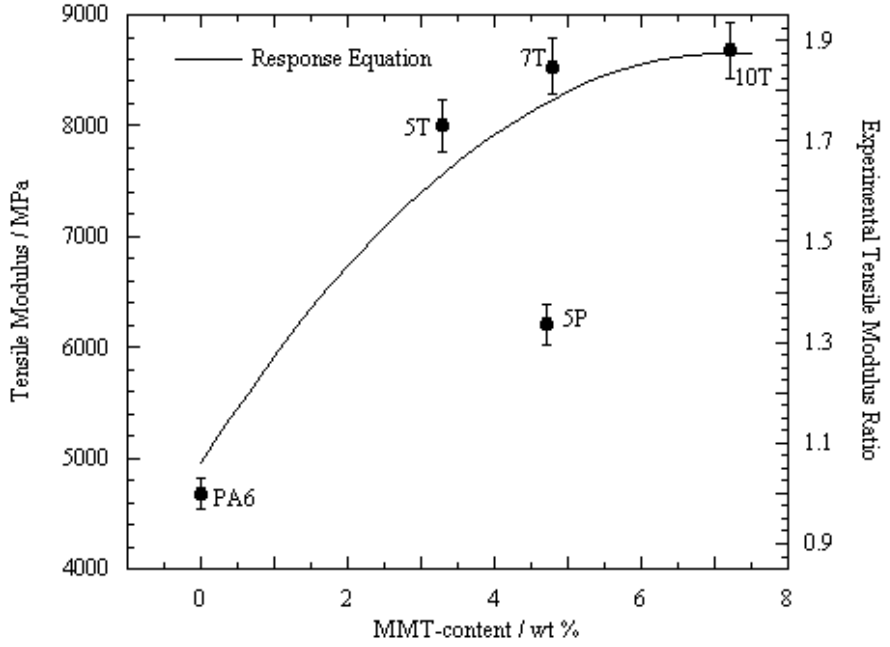

Fig 2

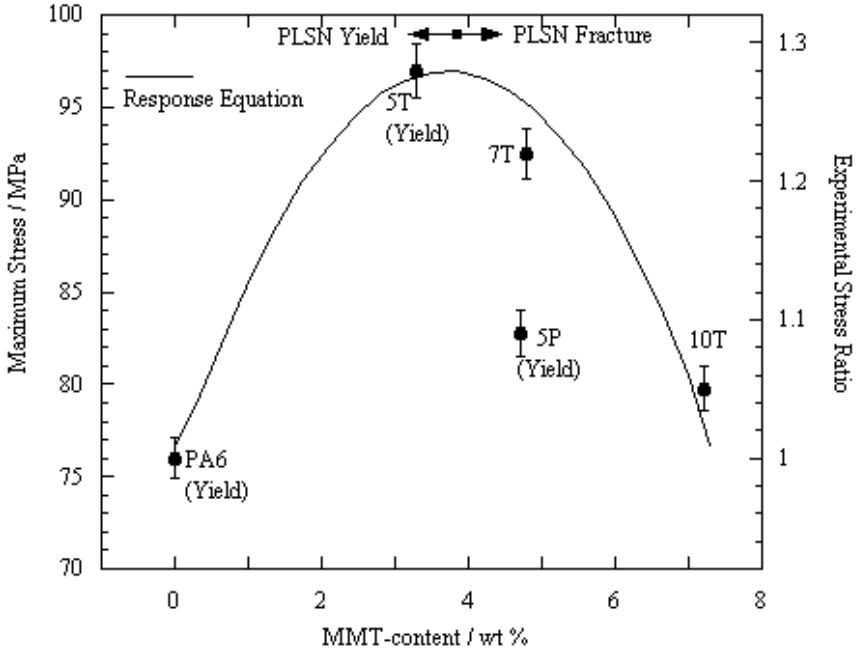

Fig 3

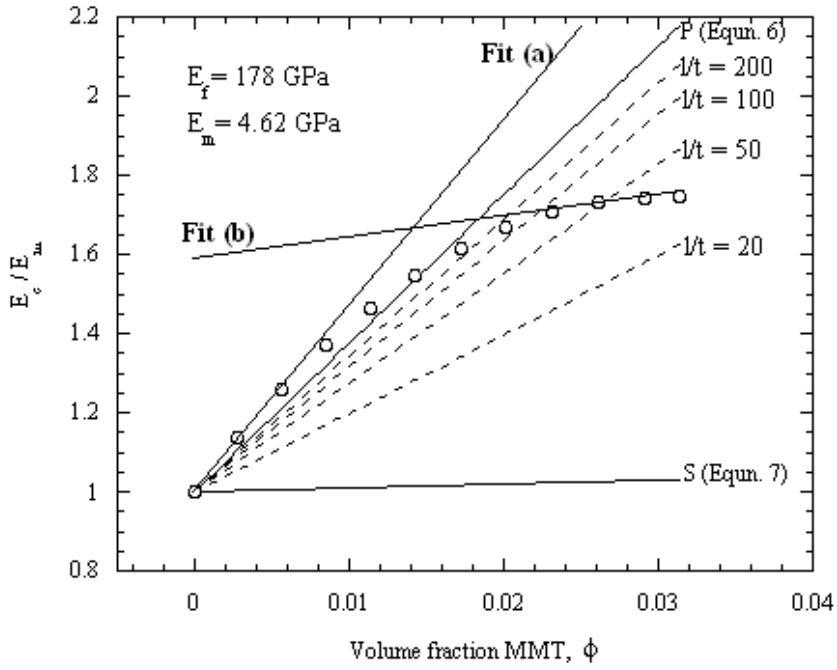

Fig 4

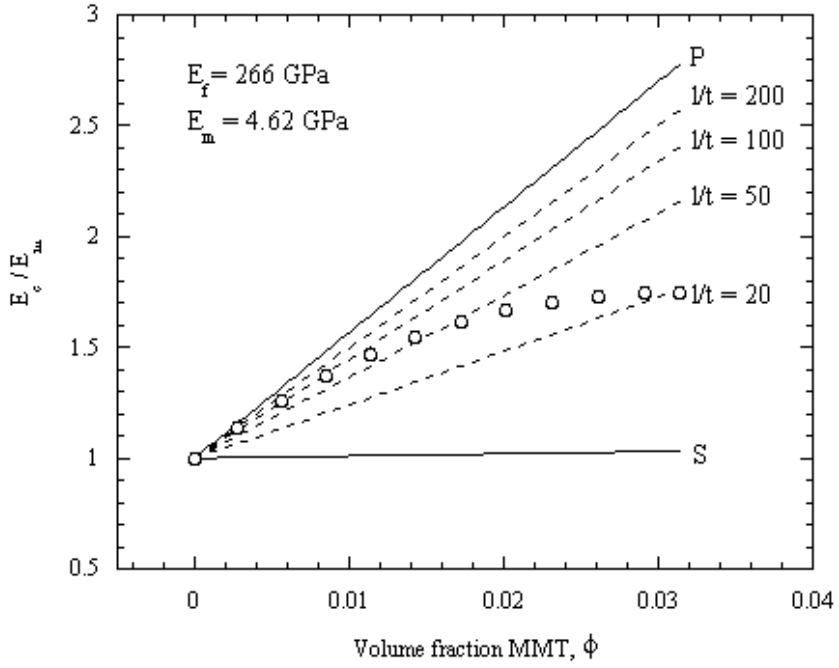

Fig 5

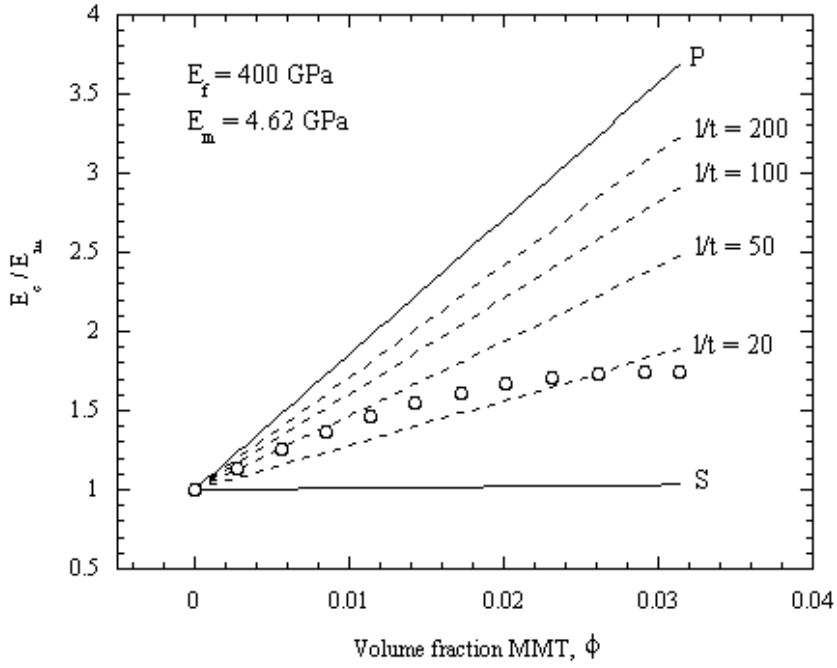

Fig 6

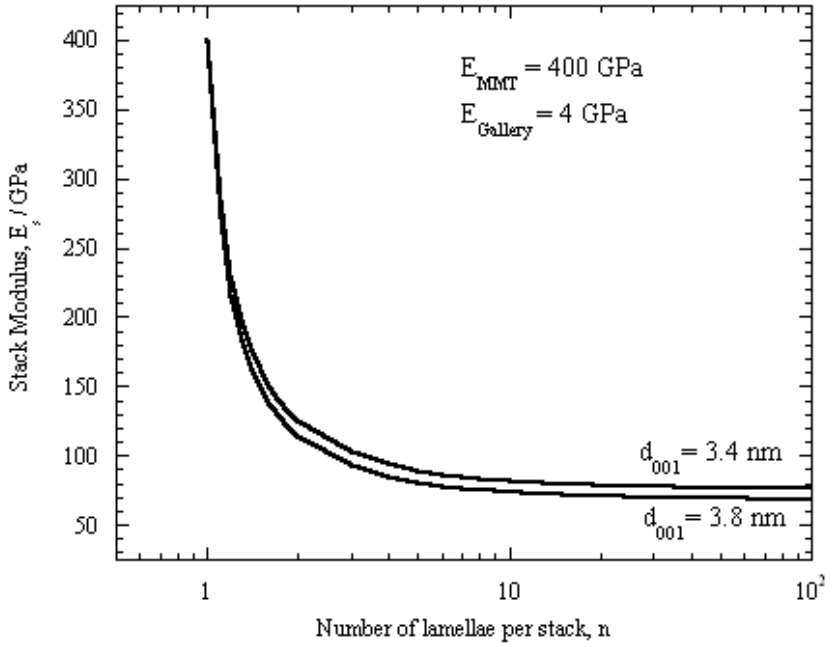

Fig 7

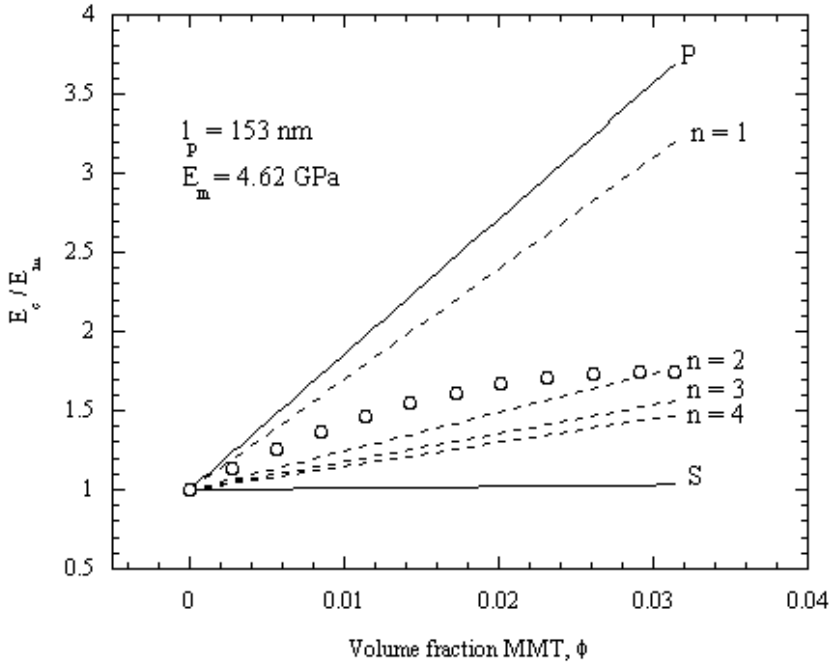

Fig 8